Title
CMIP5 model simulations of the impacts of the two types of El Niño on the U.S. winter temperature

Authors
Zou, Yuhao
Yu, Jin-Yi
Lee, Tong
et al.

Publication Date
2014-03-01

DOI
10.1002/2013JD021064

Peer reviewed

AGU PUBLICATIONS

JGR

Journal of Geophysical Research: Atmospheres

RESEARCH ARTICLE
10.1002/2013JD021064

Key Points:
- CMIP5 models simulate U.S. winter response to EP ENSO well but not to CP ENSO
- The performance difference is due to different OLR response induced by two ENSOs
- The two types of ENSO initiate different wavetrain patterns in the NH

Correspondence to:
J.-Y. Yu,
jyyu@uci.edu

Citation:
Zou, Y., J.-Y. Yu, T. Lee, M.-M. Lu, and S. T. Kim (2014), CMIP5 model simulations of the impacts of the two types of El Niño on the U.S. winter temperature, *J. Geophys. Res. Atmos.*, *119*, doi:10.1002/2013JD021064.

Received 20 OCT 2013
Accepted 22 FEB 2014
Accepted article online 27 FEB 2014

CMIP5 model simulations of the impacts of the two types of El Niño on the U.S. winter temperature

Yuhao Zou[1], Jin-Yi Yu[1], Tong Lee[2], Mong-Ming Lu[3], and Seon Tae Kim[4]

[1]Department of Earth System Science, University of California, Irvine, California, USA, [2]Jet Propulsion Laboratory, California Institute of Technology, Pasadena, California, USA, [3]Research and Development Center, Central Weather Bureau, Taipei, Taiwan, [4]Marine and Atmospheric Research, CSIRO, Aspendale, Victoria, Australia

Abstract Thirty Coupled Model Intercomparison Project phase 5 (CMIP5) preindustrial simulations are examined to contrast impacts of the two types of El Niño on the U.S. winter temperatures. The CMIP5 models are found more capable of simulating the observed eastern Pacific (EP) El Niño impacts (a warm northeast, cold southwest pattern over the U.S.) but less capable of simulating the observed central Pacific (CP) El Niño impacts (a warm northwest, cold southeast pattern). During EP El Niño, sea surface temperature (SST) anomalies influence the Walker circulation giving rise to a basin-wide pattern of outgoing longwave radiation (OLR) anomalies. The modeled atmospheric responses to the EP El Niño are thus less sensitive to the detailed structure of the simulated SST anomalies and can be well simulated by most of the CMIP5 models. In contrast, the SST anomalies during the CP El Niño affect the strength of the Walker circulation less effectively than the EP El Niño. OLR anomalies are local, rather than basin wide. The modeled atmospheric responses to the CP El Niño therefore depend more on how realistically the CP El Niño SST anomalies are simulated in the models. As a result, the CP El Niño's impact on the U.S. winter temperature, controlled by the atmospheric wave train response to the OLR forcing, is less well simulated by the CMIP5 models. This conclusion is supported by an examination of the Pacific North American and tropical/Northern Hemisphere patterns produced by the CMIP5 models in response to the two types of El Niño.

1. Introduction

The impacts of El Niño on the United States (U.S.) climate have been extensively studied over the past few decades [e.g., *Ropelewski and Halpert*, 1986, 1989; *Kiladis and Diaz*, 1989; *Livezey et al.*, 1997; *Dettinger et al.*, 1998; *Mo and Higgins*, 1998; *Montroy et al.*, 1998; *Cayan et al.*, 1999; *Larkin and Harrison*, 2005, and many others]. For the winter climate, El Niño's impact has traditionally been described as a north-south anomaly pattern with the winter being colder and wetter than normal in the southern U.S. and warmer and drier than normal in the northern U.S. This conventional view has been revised in recent years amid the increasing recognition that there exist different types or flavors of El Niño events [*Larkin and Harrison*, 2005; *Ashok et al.*, 2007; *Yu and Kao*, 2007; *Guan and Nigam*, 2008; *Kao and Yu*, 2009; *Kug et al.*, 2009]. Two particular types have been emphasized: an eastern Pacific (EP) type that has its sea surface temperature (SST) anomalies located off the South American coast and a central Pacific (CP) type that has the anomalies confined around the International Date Line [*Yu and Kao*, 2007; *Kao and Yu*, 2009]. *Weng et al.* [2009], for example, noticed that EP El Niño events increase rainfall in the western U.S. by shifting the polar jet stream equatorward, while CP El Niño events increase the rainfall there by shifting the Intertropical Convergence Zone poleward. *Mo* [2010] contrasted the impacts of El Niño on air temperature and precipitation over the U.S. during the period 1915–1960 when the EP type dominated and the period 1962–2006 when the CP type became increasingly dominant. She noted that the EP El Niño produces a north-south contrast pattern in the U.S. winter temperature variations, while the CP El Niño produces an east-west contrast pattern. *Yu and Zou* [2013] showed that the CP El Niño enhances the typical drying effect of El Niño over the northern U.S. but weakens the wetting effect over the southern U.S. These and other recent studies [e.g., *Sheffield et al.*, 2013; *Xu et al.*, 2013; *Liang et al.*, 2014] support the assertion that the EP and CP El Niño have different impacts on the U.S. climate.

Yu et al. [2012b] developed a way to identify the El Niño impacts of the two types using two indices that they called CP and EP indices. By regression analyses with these two indices, they showed that the El Niño impact

Table 1. The Full Names and Abbreviations of the 30 Selected CMIP5 Models

A–J	K–T	U–d
A:ACCESS1 – 0	K:CMCC – CESM	U:inmcm4
B:ACCESS1 – 3	L:CMCC – CM	V:IPSL – CM5A – LR
C:bcc – csm1 – 1	M:CMCC – CMS	W:IPSL – CM5A – MR
D:bcc – csm1 – 1 – m	N:CSIRO – Mk3 – 6 – 0	X:IPSL – CM5B – LR
E:CanESM2	O:GFDL – CM3	Y:MIROC5
F:CCSM4	P:GFDL – ESM2G	Z:MPI – ESM – LR
G:CESM1 – BGC	Q:GFDL – ESM2M	a:MPI – ESM – P
H:CESM1 – CAM5	R:GISS – E2 – H	b:MRI – CGCM3
I:CESM1 – FASTCHEM	S:HadGEM2 – CC	c:NorESM1 – M
J:CESM1 – WACCM	T:HadGEM2 – ES	d:NorESM1 – ME

pattern on the U.S. winter temperature is rotated by 90° between these two types of El Niño. During the EP El Niño, warm surface air temperature anomalies appear in the northeastern U.S., while cold anomalies appear in the southwestern US. During the CP El Niño, the winter warm anomalies are located in the northwestern U.S. and the cold anomalies in the southeastern U.S. These contrasting impact patterns are close to those reported in the composite study of *Mo* [2010] but with some additional details in the spatial structures. *Yu et al.* [2012b] showed that these two impact patterns can be reproduced in the Center for Atmospheric Research (NCAR)'s Community Atmospheric Model (CAM) version 4 when the model was forced by the sea surface temperature anomalies representative of the two types of El Niño. Furthermore, *Yu et al.* [2012b] were able to show that these two impact patterns can be identified in individual CP and EP El Niño events observed during 1950–2010. Therefore, the different impact patterns reported by *Yu et al.* [2012b] between the two types of El Niño on U.S. winter temperature are robust. Both *Mo* [2010] and *Yu et al.* [2012b] linked the different impact patterns to different planetary wave train patterns in the extratropical atmosphere. They are consistent in showing that the CP El Niño is associated more with a positive phase of the Pacific North America (PNA)[*Wallace and Gutzler*, 1981] pattern, and the EP El Niño is associated more with a poleward propagating wave train that resembles the negative phase of tropical Northern Hemisphere (TNH)[*Mo and Livezey*, 1986] pattern. The PNA pattern is characterized by geopotential height anomalies that spread eastward and poleward from the tropical Pacific to Alaska and Canada and then reflect equatorward through the U.S. *Yu et al.* [2012b] showed that the PNA pattern over the U.S. domain consists of positive geopotential height anomalies over the northwest U.S. and negative geopotential height anomalies over the southeast U.S. during CP El Niño. A warm northwest, cold southeast impact pattern is thus produced in the U.S. winter during CP El Niño events. Associated with the TNH pattern, the EP El Niño events excite a wave train characterized by negative geopotential height anomalies over the southwest U.S. and positive geopotential height anomalies over the northeast U.S. This geopotential height anomaly pattern leads to a warm northeast, cold southwest pattern in the U.S. winter temperatures during the EP El Niño. Therefore, the extratropical atmosphere responds to the two types of El Niño with two distinct wave train patterns, which results in different impact patterns on the U.S. winter climate.

This study examines whether the Coupled Model Intercomparison Project phase 5 (CMIP5) models can simulate the different impacts of the two types of El Niño on the U.S. winter temperature. The model performance is expected to depend on two factors: (1) how well the two types of El Niño are simulated and (2) how realistically the model atmospheres respond to the different forcing produced by the two types of El Niño. In order to investigate these factors, we examine not only the tropical Pacific SST and U.S. winter temperature patterns associated with the two types of El Niño but also their associated outgoing longwave radiation (OLR) anomalies and atmospheric planetary wave trains. This paper is organized as follows: The data sets used in this study are described in section 2. The model simulations of the two types of El Niño are presented in section 3. The U.S. winter temperature responses to El Niño in the CMIP5 models are examined in section 4. Relations among SST, OLR, and U.S. air temperature are investigated in section 5. The modeled wave train patterns are compared to reanalysis results in section 6. A summary and discussion of the results follows in section 7.

2. Observational and CMIP 5 Model Data Sets

This study uses three observation/reanalysis data products: (1) the SST data from the National Oceanic and Atmospheric Administration (NOAA)'s Extended Reconstructed Sea Surface Temperature v3b data set

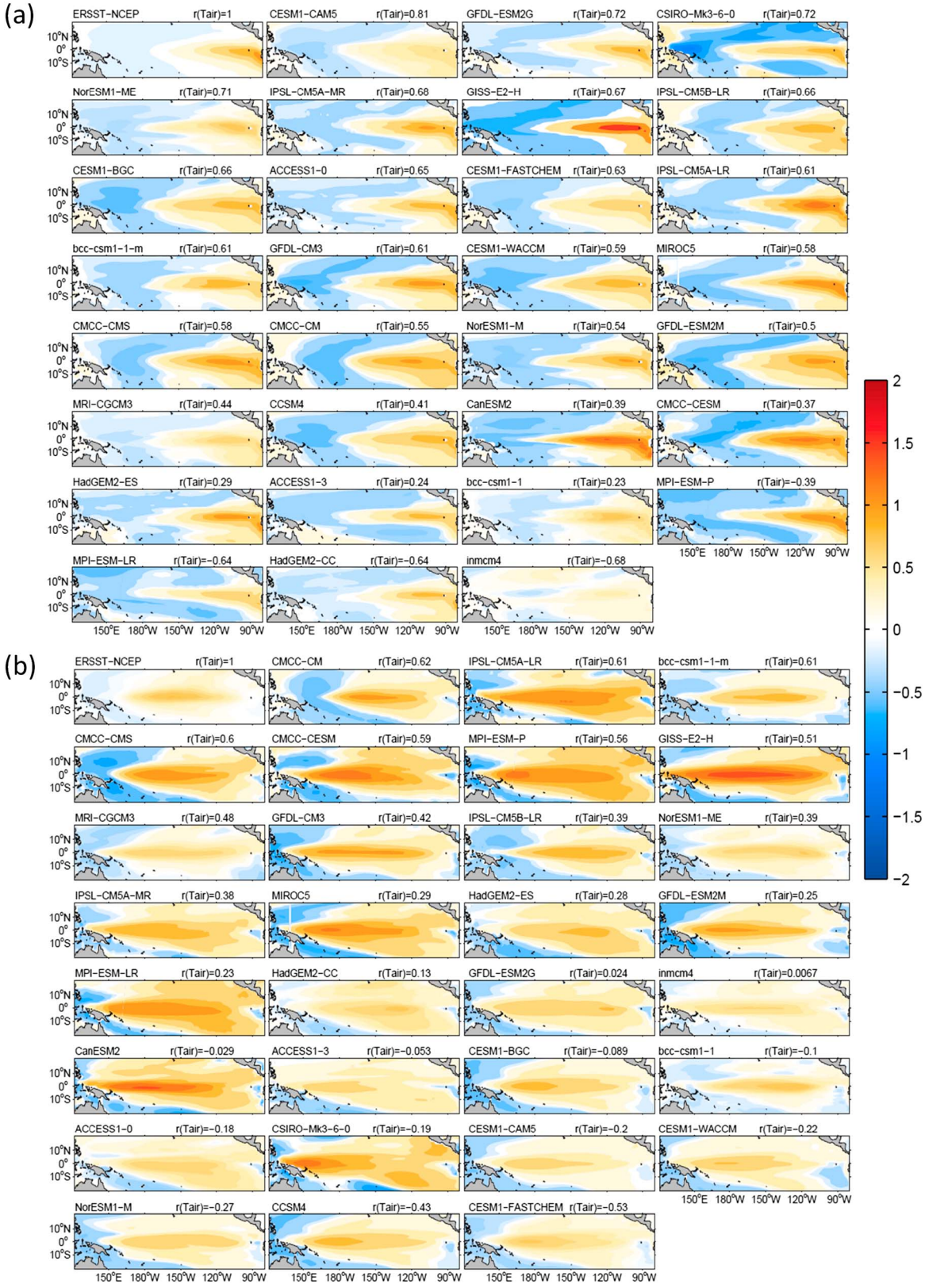

Figure 1. The EOF patterns of SST anomalies calculated from the observations and the CMIP5 models for (a) EP El Niño and (b) CP El Niño. The loading coefficients in the patterns have been scaled by their corresponding eigenvalues to reflect their amplitudes and are in the units of degree Celsius. The patterns are shown in order from the highest to lowest pattern correlation between the observations and modeled U.S. winter air temperature regression patterns (see Figure 5).

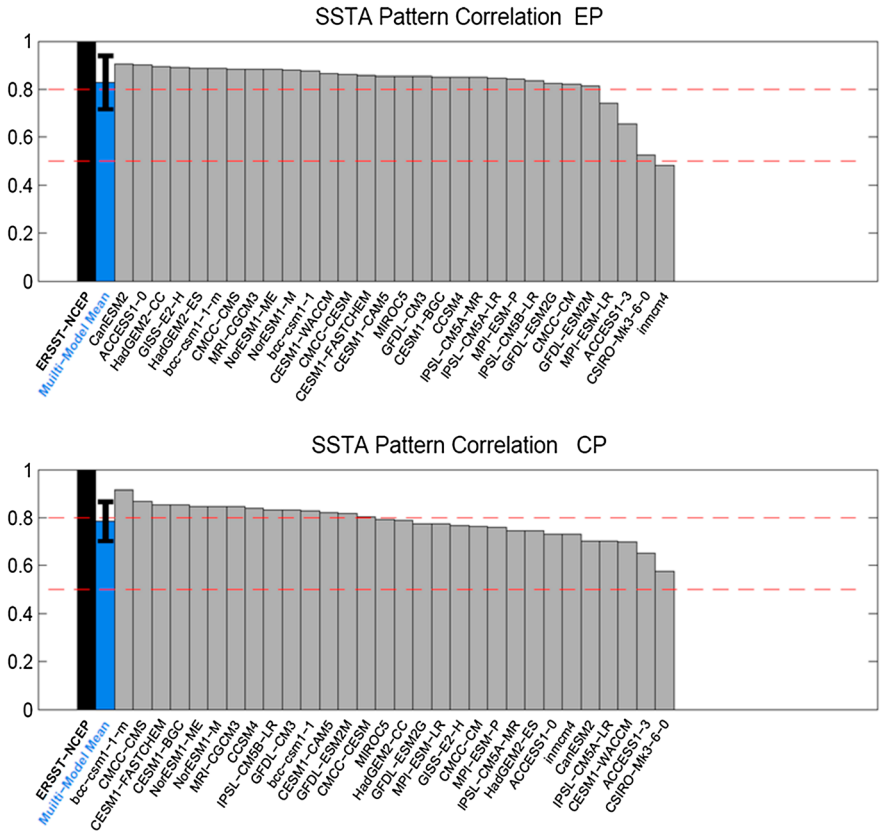

Figure 2. The pattern correlations between the observed and model SST anomaly patterns for the (top) EP El Niño and (bottom) CP El Niño, ordered from the highest to lowest values. The anomaly patterns are the scaled loading patterns from the EOF analysis (see Figure 1). The multimodel mean (blue) is also shown with its spread (defined by 1 standard deviation of the multimodel values) indicated by a black line.

[*Smith and Reynolds*, 2003] with a 2° × 2° resolution, available from January 1854; (2) the near-surface air temperature and geopotential height data from the National Centers for Environmental Prediction–National Center for Atmospheric Research (NCEP-NCAR) Reanalysis [*Kalnay et al.*, 1996] with a 2.5° × 2.5° resolution, available from January 1948; and (3) the NOAA interpolated OLR [*Liebmann and Smith*, 1996] data set with a 2.5° × 2.5° resolution, available from June 1974. Monthly SST, geopotential height, and air temperature anomalies from 1948 to 2010 were analyzed. The anomalies are defined as the deviations from the 1948–2010 climatology. Monthly OLR anomalies from 1975 to 2010 were analyzed. Anomalies of OLR are defined as the deviations from the 1981–2010 climatology. Also used in this analysis are the winter values of the PNA index and TNH index during 1950–2010 downloaded from the Climate Prediction Center of NOAA.

We focus our analyses on the preindustrial simulations produced by 30 CMIP5 models (see Table 1). The length of the preindustrial simulations varies from model to model. Five hundred years of each simulation are analyzed in this study. We choose to analyze the preindustrial simulations because their integration lengths are longer than those of the historical simulations. The preindustrial simulations and historical simulations of CMIP5 (19th, 20th, and 21st century) have almost the same intensity ratios of CP/EP El Niño, although the historical simulations have slightly higher intensity [*Kim and Yu*, 2012].

Following *Yu et al.* [2012b], the anomalies associated with the two types of El Niño were identified by regressing the corresponding fields onto the EP and CP indices. The monthly values of the EP and CP indices were calculated separately by applying a regression-empirical orthogonal function (EOF) analysis [*Kao and Yu*, 2009; *Yu and Kim*, 2010] to both the observed and simulated SST anomalies. In this method, the SST anomalies regressed with the Niño1 + 2 (0°S–10°S, 80°W–90°W) SST index were considered as the influence from the EP El Niño and were removed before the EOF analysis was applied to identify the spatial pattern of the CP El Niño. Similarly, the SST anomalies regressed with the Niño4 (5°S–5°N, 160°E–150°W) index were considered as the

influence from the CP El Niño and were removed before the EOF analysis was applied to identify the leading structure of the EP El Niño. The principal components of the leading EOF modes for the EP and CP El Niño represent the temporal variations of these two types of El Niño and are referred to as the EP index and the CP index, respectively.

3. Simulation of the Two Types of El Niño in CMIP5 Models

Figure 1 shows the SST anomaly patterns of the two types of El Niño identified by the regression-EOF method from the 30 CMIP5 models and the observations. Here the loading coefficients of each EOF mode have been scaled by the square root of their eigenvalues to reflect the standard deviation of the SST anomalies associated with the mode [*Yu and Kim*, 2010]. The intensity of the El Niño can therefore be quantified as the maximum value of the scaled loading coefficient. The figure shows that the simulated EP El Niños have positive SST anomalies in the eastern Pacific near the South American coast, with some variations in the intensity and central location of the anomalies. The simulated CP El Niños have positive SST anomalies located over a wider range of longitudes with varying intensities and areas covered. This is reflected in the values of the pattern correlations between the simulated and observed SST anomalies shown in Figure 2 for these two types of El Niño. For the EP El Niño, 26 models have pattern correlations larger than 0.8. For the CP El Niño, only 14 models have correlations larger than 0.8. Nevertheless, most of the CMIP5 models can reproduce the two types of El Niño with reasonable spatial structures. Almost all the models produce pattern correlations larger than 0.5 for the two types of El Niño. The pattern correlation of the multimodel mean is around 0.8 for both types of El Niño, and the spreads (defined by 1 standard deviation of the multimodel values) do not include pattern correlations smaller than 0.6. It is concluded that the two types of El Niño can be identified in the CMIP5 models.

4. U.S. Winter Temperature Response to El Niño in CMIP5 Models

Following *Yu et al.* [2012b], the U.S. winter (January-February-March: JFM) near-surface air temperature anomalies are regressed onto the EP and the CP indices for the preindustrial simulations and the observations. The regression coefficients are shown in Figures 3 and 4. In the figures, only the model points that pass the 10% significance level using the Student's *t* test or the observational points that have values greater than 0.1 are plotted. For the observations, the regressions are characterized by a warm northeast, cold southwest pattern for the EP El Niño and a warm northwest, cold southeast pattern for the CP El Niño, as reported by *Yu et al.* [2012b]. As mentioned, these two contrasting patterns were confirmed by *Yu et al.* [2012b] by numerical experiments and case studies, and the differences in the patterns are robust. In Figures 3 and 4, the regressed U.S. anomaly patterns from the CMIP5 models are arranged from the highest pattern correlation with the observed impact pattern to the lowest. The pattern correlations reflect the structure similarity between model and observed regression patterns. It is noticed from Figure 3 that the U.S. winter responses to the EP El Niño are reasonably simulated by most of the CMIP5 models. The pattern correlation for the "best" model (Community Earth System Model (CESM1-CAM5)) is as high as 0.81, and the pattern correlations are still very high for most of the lower ranked models. For example, the pattern correlation is still above 0.5 even for the nineteenth-ranked CMIP5 model. The warm northeast, cold southwest pattern can be seen in many of the CMIP5 models. However, the situation is quite different for the CP El Niño. As shown in Figure 4, the pattern correlation drops below 0.5 quickly after the seventh-ranked model. The observed warm northwest, cold southeast pattern can only be found in the top few best models. In some of the CMIP5 models, the U.S. winter responses to the CP El Niño are even opposite from that observed (e.g., CCSM4 and CESM1-FASTCHEM). Figures 3 and 4 therefore indicate that the CMIP5 models are more capable of realistically simulating the U.S. winter temperature impact produced by the EP El Niño than the impact produced by the CP El Niño.

The different performances of the CMIP5 models in simulating the U.S. temperature responses to the two types of El Niño can be further demonstrated in Figure 5, where the pattern correlations calculated between the simulated and the observed U.S. winter temperature anomaly regressions are ranked from the highest to the lowest values. Figure 5 shows that for the impact pattern produced by the EP El Niño, 19 of the 30 CMIP5 models produce pattern correlations larger than 0.5. Only 4 models produce negative pattern correlations. In contrast, for the impact pattern produced by the CP El Niño, only 7 out of the 30 models have pattern

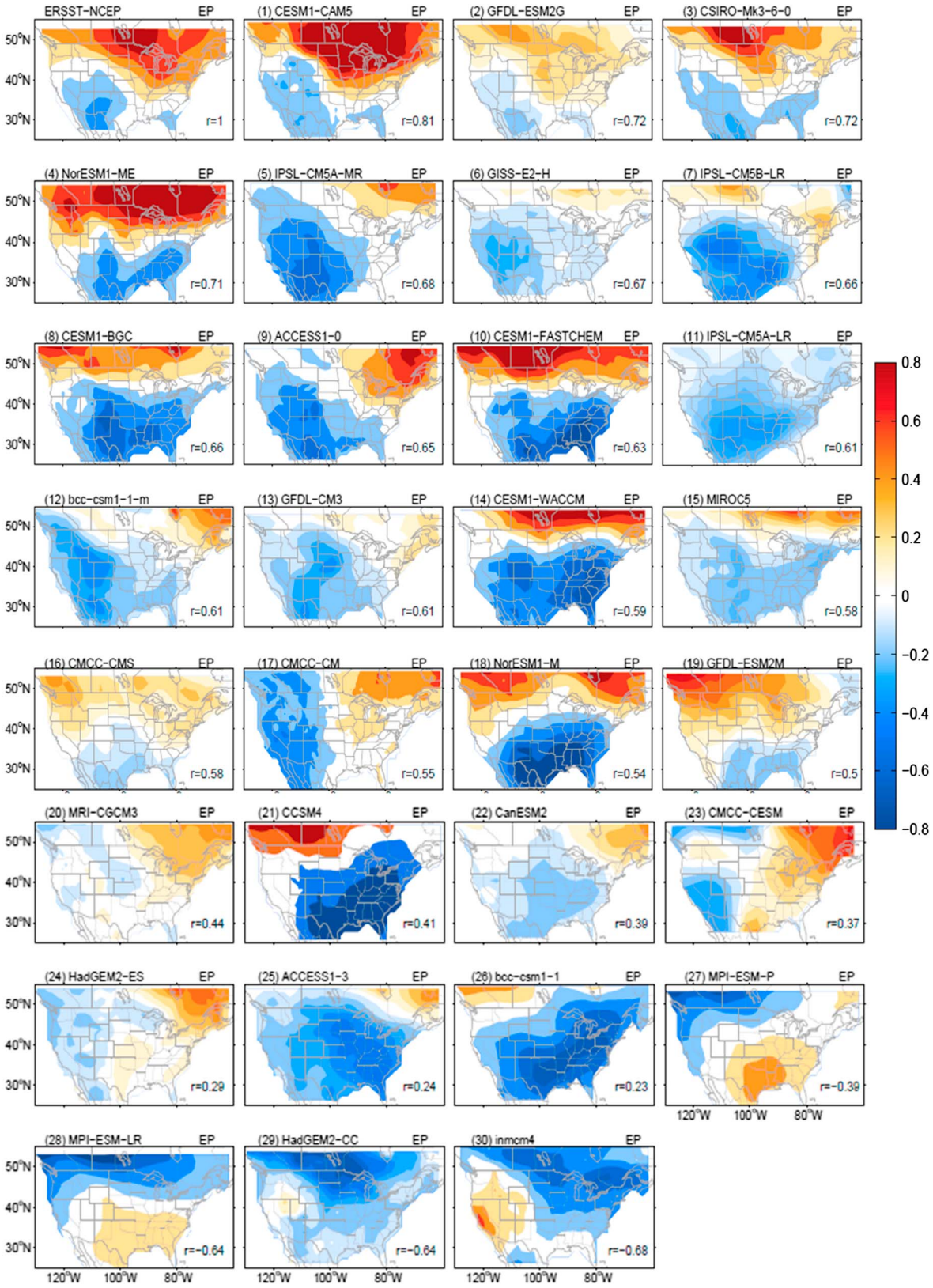

Figure 3. The regression patterns of the U.S. winter near-surface air temperature anomalies on the EP index calculated from the observations and the CMIP5 models. Values shown are in the units of degree Celsius per standard deviation, in order from the highest to lowest pattern correlation (*r*) between the observed and modeled regression patterns.

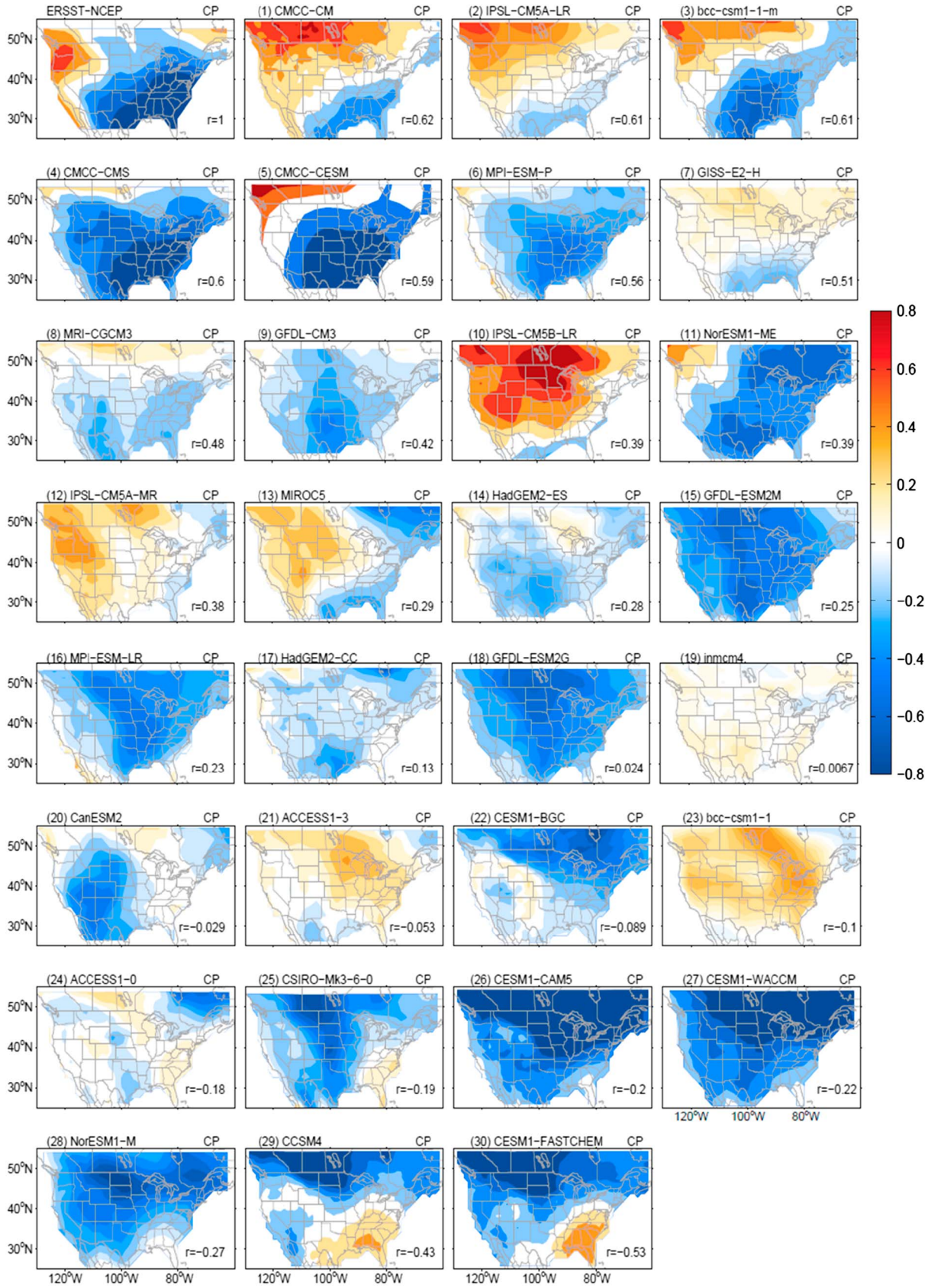

Figure 4. Same as Figure 3 but for the CP El Niño.

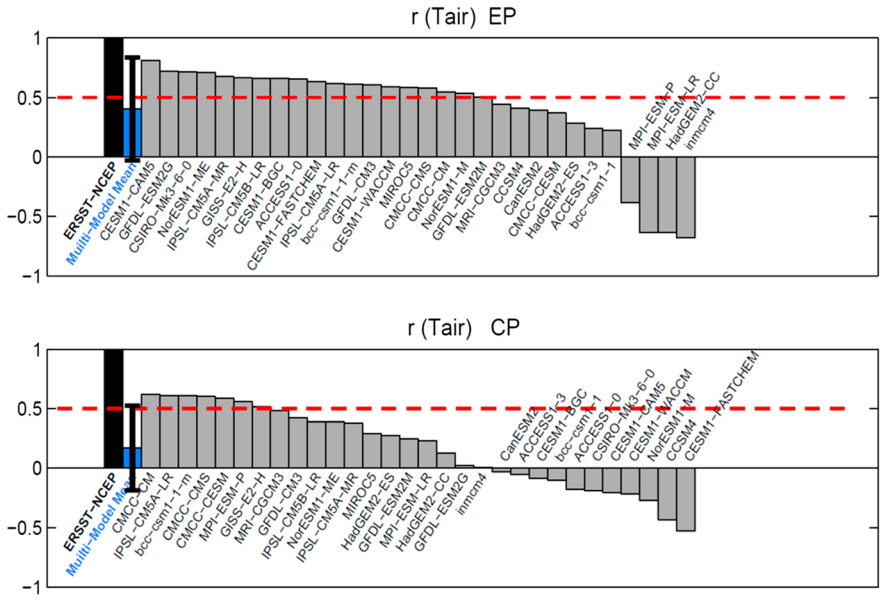

Figure 5. Values of the pattern correlations between the observed and modeled U.S. winter air temperature anomalies for the (top) EP El Niño and (bottom) CP El Niño, ordered from the largest to the smallest. The multimodel means (blue) are also shown with their spreads indicated by black lines.

correlations larger than 0.5. Eleven CMIP5 models produce negative pattern correlations. The multimodel means and spreads shown in the figure also indicate that the impact simulation is more realistic for the EP El Niño than for the CP El Niño. In the next section, we will analyze why there exists such a difference in the model performance. It is necessary to mention that the pattern correlations calculated between the model and observations can be influenced by the uncertainties in the observed regression patterns and that the smaller mean pattern correlation for the CP El Niño may be partly due to larger uncertainties in the observed impact pattern of the CP El Niño. This possibility will have to be addressed when longer observational data sets become available.

5. Relationships Among SST, OLR, and U.S. Responses

Heating associated with deep convection is one key process by which El Niño influences the atmosphere. The intensity and location of deep convection can be represented by the OLR. The importance of using OLR anomalies to understand the atmospheric teleconnections from the tropics had been emphasized in many earlier studies [e.g., *Heddinghaus and Krueger*, 1981; *Lau and Chan*, 1983, 1985; *Gruber and Krueger*, 1984; *Ardanuy and Kyle*, 1986; *Chiodi and Harrison*, 2013]. In order to understand why it is relatively easier for the CMIP5 models to simulate the U.S. winter response to the EP El Niño than the response to the CP El Niño, we need to look into the OLR anomalies induced by the two types of El Niño and examine how well the OLR anomalies are simulated in CMIP5 models. For this purpose, we regressed OLR anomalies on the EP and CP indices. Due to the limited length of the OLR data set, the regression was conducted only for the period 1975–2010. To make sure that this OLR analysis can be used to explain the different U.S. impact patterns discussed in section 4 for the two types of El Niño, we repeated the same regression analyses for the U.S. winter impact pattern using this shorter period. Similar patterns (not shown) were obtained as those shown in Figures 3 and 4. Figure 6 shows that when regressed with the EP index, the negative OLR anomalies (i.e., enhanced deep convection) are observed to spread from the eastern equatorial Pacific to the central-western equatorial Pacific, covering almost the entire basin. Similar basin-wide OLR anomalies can be seen in many of the CMIP5 models (at least the first 20 models in the figure). This can explain why many of the CMIP5 models are able to reasonably simulate the observed U.S. winter temperature response pattern to the EP El Niño. So why then do the real-world atmosphere and many of the CMIP5 models show similar basin-wide patterns of OLR anomalies in association with the EP El Niño? As shown in Figure 1a, the

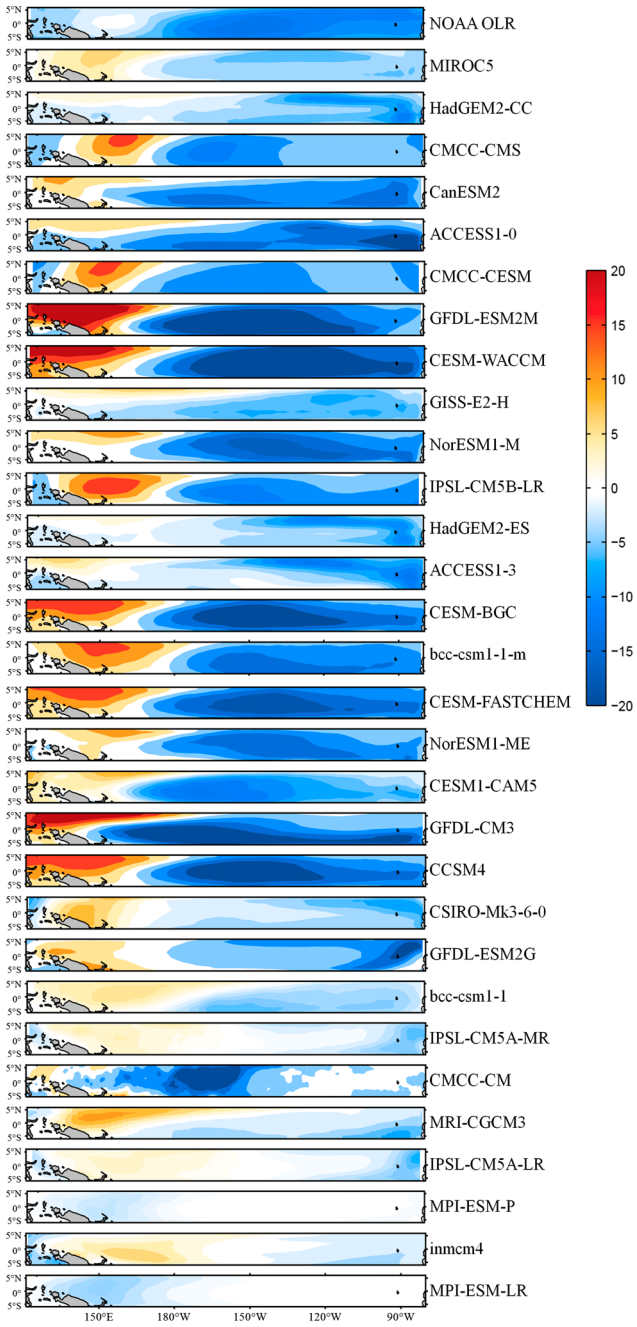

Figure 6. The regression patterns of OLR anomalies on the EP index calculated from the observations and the CMIP5 models, ordered from the highest to lowest pattern correlation between the observed and modeled OLR regression patterns. Values shown are in units of W/m^2 per standard deviation.

SST anomalies associated with the observed and simulated EP El Niño are confined mostly to the eastern Pacific, where the sinking branch of the Walker circulation resides. Therefore, positive SST anomalies associated with the EP El Niño can efficiently weaken the Walker circulation to give rise to remote OLR anomalies across the basin.

In contrast, the observed OLR anomalies regressed with the CP El Niño (Figure 7) do not show a basin-wide pattern. The observed OLR anomalies are confined locally in the western Pacific. This local, rather than basin-wide, response in the OLR can be explained from the SST anomaly structure of the CP El Niño.

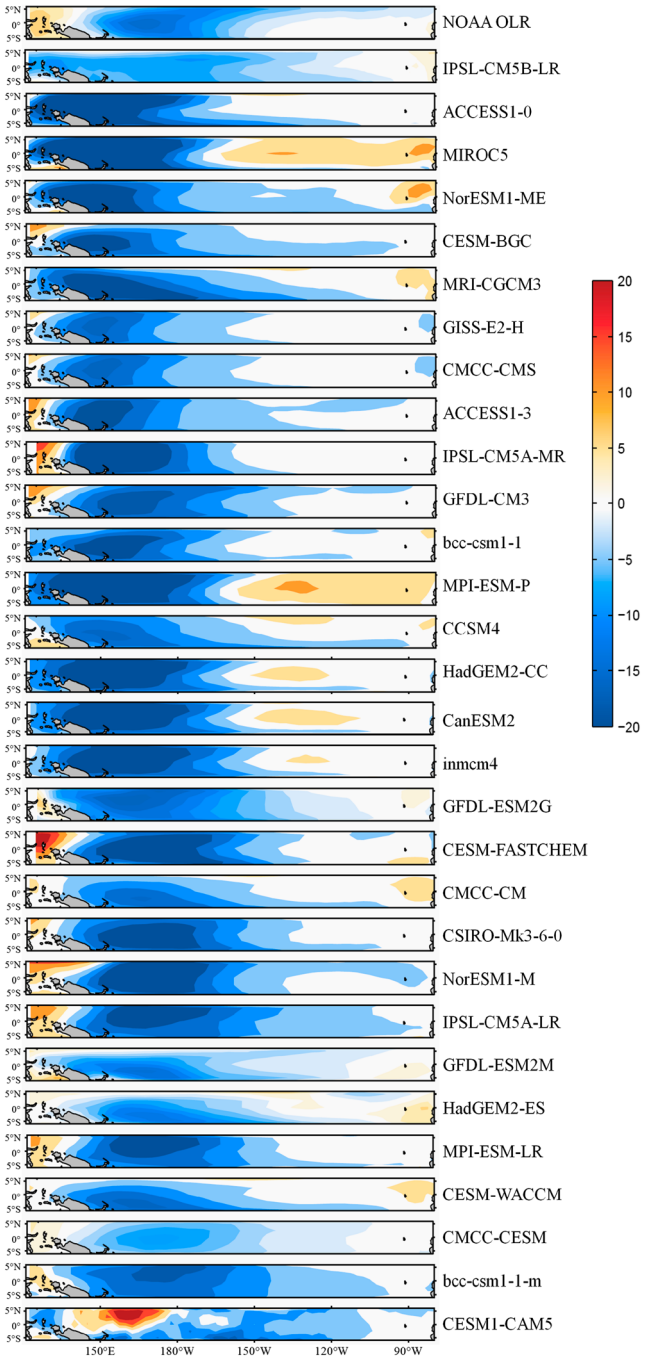

Figure 7. Same as Figure 6 but for the CP El Niño. The patterns are ordered by the locations of the maximum OLR responses (most negative values), from the westernmost to the easternmost.

As shown in Figure 1b, the SST anomalies for this type of El Niño are located mostly in the central Pacific, which does not coincide with either the sinking or the rising branch of the Walker circulation. Likely as a result of this, the SST anomalies of the CP El Niño do not induce basin-wide OLR variations but only local OLR anomalies immediately to their west. In the CMIP5 models, the OLR anomalies regressed with their simulated CP El Niño indices are also found to be confined locally to the west of the SST anomalies (cf. Figure 7 and Figure 1b). Due to the local nature of the anomalies, the OLR anomalies induced by the CP El Niño vary substantially from model to model in terms of their exact

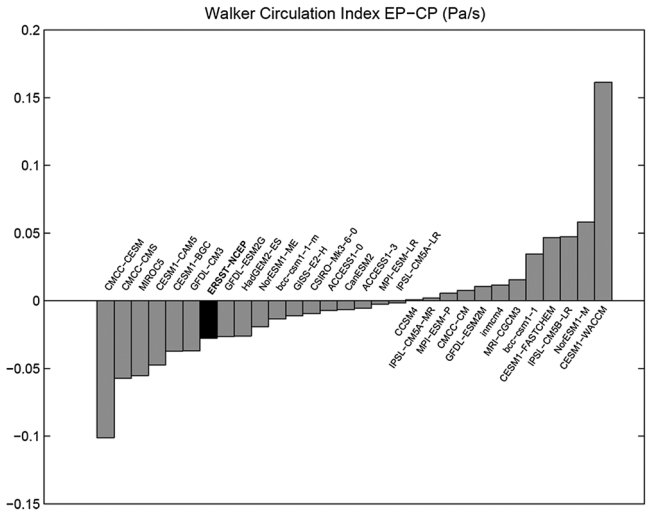

Figure 8. Differences in the Walker circulation index during EP El Niño and CP El Niño for the CMIP5 models and the observations. The Walker circulation index (see text for its definition) is calculated from the regressed 500 mb vertical velocity on the EP and CP indices. The bars are shown in units of Pa/s and are ordered from the smallest to the largest values of the index difference. There is no value for HadGEM2-CC due to its lack of 500 mb vertical velocity output.

location and size/shape. For example, the location of the OLR response varies from around 150°E in the CMIP5 models shown in the first column of Figure 7 to around 150°W in the models shown in the second column of the figure. A study by *Barsugli and Sardeshmukh* [2002] has shown that the atmosphere is most sensitive to the SST anomalies located near and around the Niño4 region (between 150°W and 150°E), which is exactly the region where the CP El Niño-induced OLR anomalies are produced in the CMIP5 models. Errors in the OLR simulations in this region can more easily cause errors in the model simulations of the atmospheric response. This higher sensitivity of the atmosphere to the details of the El Niño-induced OLR anomalies can explain why it is more challenging for the CMIP5 models to simulate the U.S. winter temperature response to the CP El Niño. Several other studies [*Simmons et al.*, 1983; *Ting and Sardeshmukh*, 1993; *Johnson and Feldstein*, 2010; *Lin et al.*, 2010] have also pointed out that the atmosphere is most sensitive to forcing located near a nodal point at 120°E. Since the bulk of the OLR anomalies produced by the EP El Niño are located farther away from this point (see Figure 6), the atmospheric response to this type of El Niño is thus less sensitive to how well the OLR anomaly patterns are simulated by the CMIP5 models. This can also explain why the CMIP5 models are more capable of simulating the U.S. winter response to the EP El Niño.

We use Figure 8 to further support our suggestion that SST anomalies associated with the EP El Niño are more capable of weakening the Walker circulation than the SST anomalies associated with the CP El Niño. In this figure, the strength of the Walker circulation is represented by the 500 mb vertical velocity difference between the equatorial eastern (180°W–100°W) and western (100°E–150°E) regions of the Pacific Ocean, in units of Pa/s [*Yu et al.*, 2012a]. By regressing the Walker circulation strength to the EP and CP indices and by calculating the difference between them, we find that the observed difference (the black bar in Figure 8) is negative, which means that the strength of the Walker circulation is reduced more by the EP El Niño than by the CP El Niño. This stronger weakening effect is simulated by 17 of the 30 CMIP5 models.

We also present a simple case study to further illustrate that the OLR responses largely, if not totally, depend on the location (i.e., EP/CP) of the El Niño SST anomalies. In this case study, we compare the OLR anomalies observed during the peak phases of the 1976 El Niño (in October) and the 2009 El Niño (in December). According to the "consensus El Niño methodology" presented by *Yu et al.* [2012b] using three different identification methods, the 1976 El Niño is an EP El Niño and the 2009 El Niño is a CP El Niño. As for the El Niño intensity, the 1976 EP El Niño event has a smaller maximum SST anomaly (1.8°C) than the 2009 CP El Niño event (2.5°C; see Figures 9a and 9b). For both events, OLR anomalies are observed over the Pacific between 5°S and 5°N (Figures 9c and 9d). However, the anomalies are more uniformly distributed across the basin

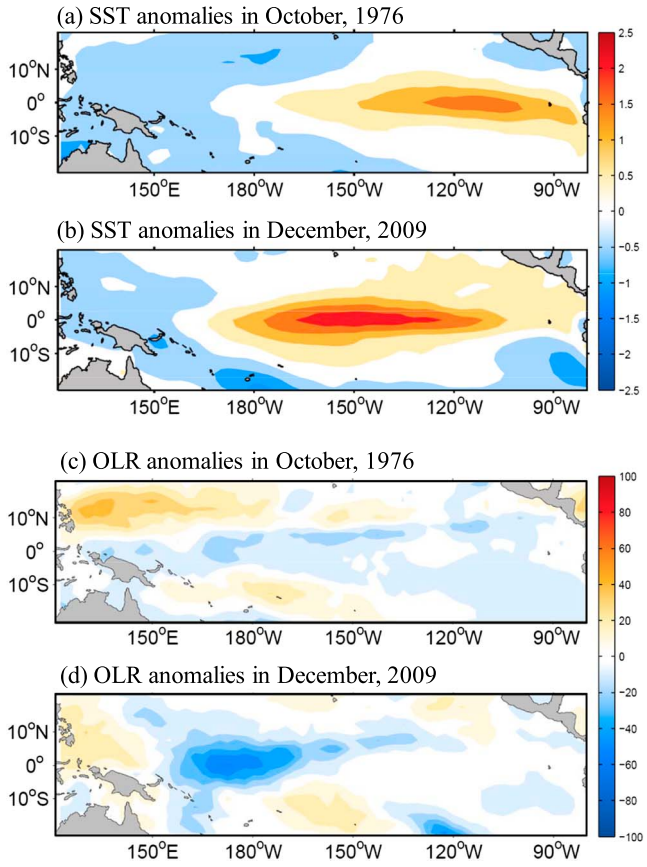

Figure 9. SST anomalies observed during the peak month of (a) the 1976 EP El Niño event and (b) the 2009 CP El Niño event. (c and d) OLR anomalies in the corresponding months. Values are in the units of degree Celsius in Figures 9a and 9b and in the units of W/m^2 in Figures 9c and 9d.

for the 1976 event but largest over the central Pacific around 180°W for the 2009 event. This case study is more-or-less consistent with our suggestion that the structure of the OLR response during El Niño events can be affected by the location of El Niño.

6. The Planetary Wave Patterns During the Two Types of El Niño

Deep convective heating excites atmospheric Rossby waves that communicate El Niño influences to higher-latitude regions including the U.S. In the Northern Hemisphere, the first four leading rotated EOF modes of 500 mb geopotential height anomalies explain about 50% of the total variance during boreal winter [*Mo and Livezey*, 1986]. Two of them are relevant to the wave trains excited by the two types of El Niño: one represents the PNA pattern and the other represents the TNH pattern. The spatial structures of these two patterns in the positive phase are shown in Figure 10 by regressing 500 mb geopotential height anomalies separately on the PNA index and TNH index obtained from NOAA. The PNA pattern (Figure 10a) has four major centers of action: (1) positive anomalies in the tropical central Pacific near Hawaii, (2) a deepened and southward displaced Aleutian low in the North Pacific, (3) positive anomalies in northwestern North America, and (4) negative anomalies in the southeast U.S. The TNH pattern (Figure 10b) also has four centers: (1) positive geopotential height anomalies along the Pacific coast of North America, (2) positive anomalies extending from the Caribbean Sea to the North Atlantic Ocean, (3) negative anomalies in east-central Canada, and (4) weak negative anomalies in the tropical central Pacific.

The observed wave train patterns associated with the two types of El Niño are shown in Figure 11, which were obtained by regressing the winter (JFM) 500 mb geopotential height anomalies from the NCEP-NCAR reanalysis onto the CP and EP indices separately. As shown, the anomalies regressed on the CP El Niño exhibit a pattern that is similar to the PNA pattern (cf. Figures 11a and 10a). For the EP El Niño, its regressed

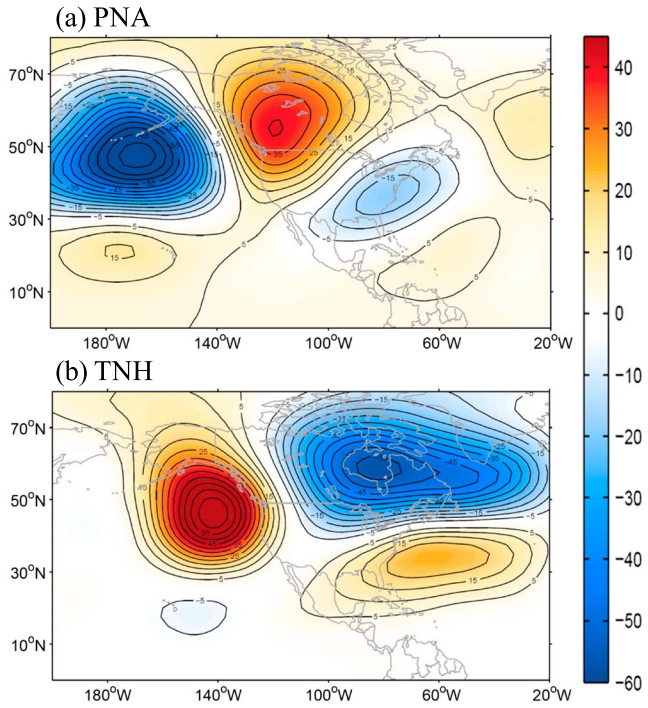

Figure 10. The 500 mb geopotential height anomalies associated with (a) the PNA pattern and (b) the TNH pattern, obtained by the regressing the anomalies on the PNA and TNH indices. Values shown are in units of meters per standard deviation.

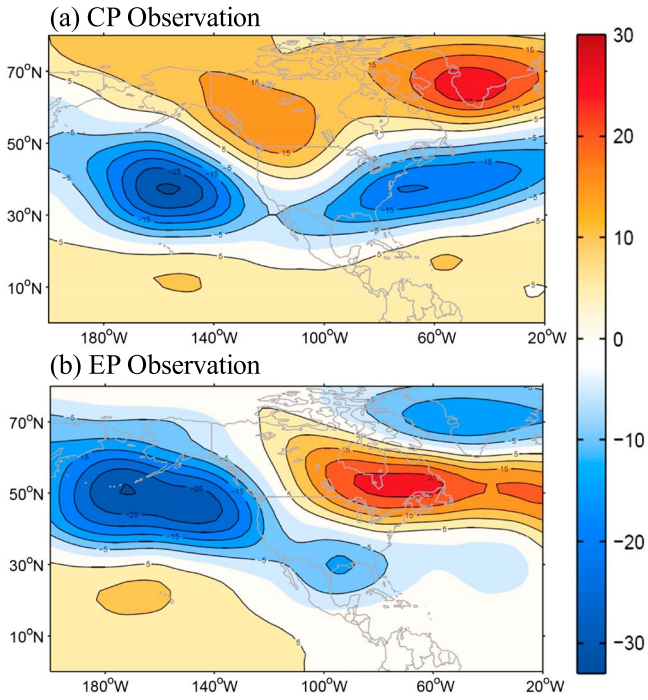

Figure 11. Regression patterns of 500 mb winter (JFM) geopotential height anomalies on (a) the CP index and (b) the EP index, calculated from the observations. Values shown are in units of meters per standard deviation.

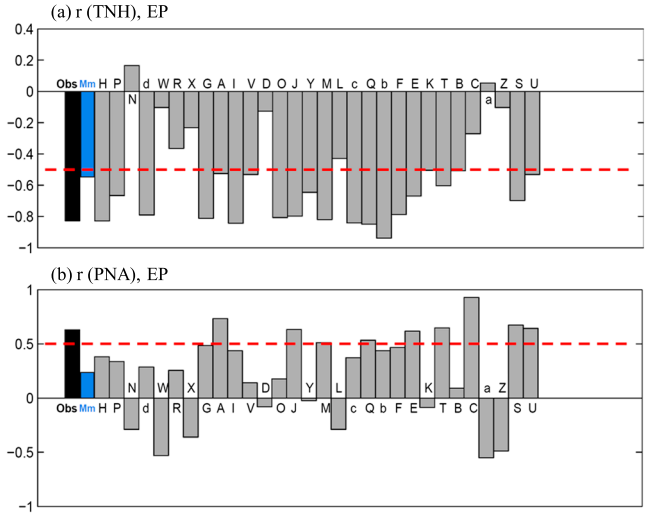

Figure 12. Pattern correlations between the winter (JFM) 500 mb geopotential height anomaly pattern regressed on the EP index, (a) the TNH pattern and (b) the PNA pattern (see Figure 10), calculated for the CMIP5 models and the observations. The multimodel means (blue) are also shown. The bars are shown ordered from the model that produces the highest pattern correlation between the observed and modeled U.S. winter air temperature regression pattern to the model that produces the lowest pattern correlation. The correspondence between the letter codes and the names of the models can be found in Table 1.

anomaly pattern resembles most closely the negative phase of the TNH pattern (cf. Figures 11b and 10b), although some discrepancies exist. Here we examine whether these two particular wave trains are also produced in the CMIP5 models for the two types of El Niño. Winter 500 mb geopotential height patterns are regressed with EP and CP indices for the 30 CMIP5 models (not shown). We then calculated the pattern correlations (within a 15°N–65°N and 180°–60°W domain) between the regressed geopotential height patterns and the observed PNA/TNH pattern shown in Figure 10. The obtained pattern correlations are shown in Figures 12 and 13. In these two figures, we display the correlations from the model that produces the most realistic U.S. winter response to the EP El Niño or CP El Niño to the model that produces the least realistic simulation of the U.S. winter response pattern. Figure 12 shows that the observed geopotential height response to the EP El Niño has a larger correlation with the TNH pattern than with the PNA pattern. Therefore, the atmospheric wave train excited by the EP El Niño in the observation resembles the negative phase of the TNH. Almost all (28 out of 30) the CMIP5 models correctly produce a negative pattern

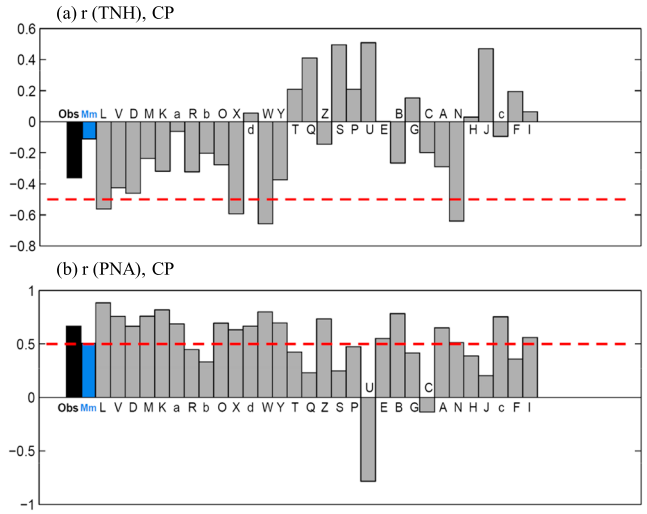

Figure 13. Same as Figure 12 but for the CP El Niño.

correlation with the TNH during their EP El Niño with the absolute value of the multimodel mean being close to 0.6, which is consistent with the fact that a majority of the CMIP5 models produce a realistic U.S. winter temperature response to the EP El Niño. The pattern correlations with the PNA are in general smaller than the pattern correlations with the TNH. The multimodel mean of the pattern correlation with the PNA is about 0.2.

As for the CP El Niño (Figure 13), the observed pattern correlation for the regressed geopotential height anomalies is larger with the PNA than with the TNH. As mentioned above, not all of the CMIP5 models are able to realistically produce the U.S. winter response to the CP El Niño. It is interesting to note from Figure 13 that most (all but two) of the models correctly produce positive pattern correlation values with the PNA, with a multimodel mean of 0.5. However, the observed negative pattern correlation with the TNH is reproduced primarily by the models that produce more realistic simulations of the U.S. winter temperature response pattern to the CP El Niño (e.g., the leftmost 13 models in Figure 13a). Among the rightmost 17 models in Figure 13a that produce less realistic simulations of the U.S. winter response to the CP El Niño, 11 of them produce positive pattern correlations with the TNH. For those models, the opposite TNH pattern becomes so large that it overwhelms the PNA pattern, degrading the model's performance in simulating the U.S. response to the CP El Niño. With an incorrect positive phase of the TNH, negative geopotential height anomalies are produced over a large part of the U.S. that cancel out or even overcome the positive anomalies associated with the positive phase of the PNA. This is the case for CESM1-WACCM (Whole Atmosphere Community Climate Model), for example (see Figure 4). Figure 13 therefore indicates that it is the erroneous simulation of the TNH in the model atmosphere that prevents a number of CMIP5 models from correctly simulating the U.S. winter temperature response to the CP El Niño.

7. Conclusions and Discussions

Using preindustrial simulations produced by 30 CMIP5 models, we examined the relationships among El Niño SST forcing, OLR responses, atmospheric wave responses, and the U.S. winter air temperature patterns for the two types of El Niño. Our primary conclusion is that the CMIP5 models are more capable of simulating the U.S. winter temperature response to the EP El Niño than the response to the CP El Niño. This difference in model performance is shown to be related to differences in the spatial pattern of OLR anomalies induced by the two types of El Niño in the equatorial Pacific, as well as the differences in the atmospheric sensitivity to the locations of the OLR anomalies. The OLR response to the EP El Niño is shown to have a basin-wide structure, while the response to the CP El Niño tends to be confined in its longitudinal extent and to be located to the west of the associated SST anomalies. This local nature of the OLR response during the CP El Niño makes the model atmosphere sensitive to the exact location of the SST (and therefore the OLR) anomalies simulated in the models. Also, the OLR anomalies induced by the CP El Niño are located more in the central-to-western Pacific, where the atmospheric response to tropical forcing is the most sensitive. Deep convection then transmits the El Niño influences to the continental U.S. by exciting planetary atmospheric wave trains. While most of the CMIP5 models realistically produce a negative phase of the TNH in response to the EP El Niño and a positive phase of the PNA in response to the CP El Niño (i.e., 26 out of the 30 models, according to Figures 12a and 13b), many CMIP5 models also erroneously produce an incorrect phase of the TNH during CP El Niño events (i.e., 12 out of 30 models, according to Figure 13a). The incorrect TNH response overpowers the correct PNA response in some models, leading to unrealistic simulations of the U.S. winter temperature response to the CP El Niño. A better understanding of the generation mechanisms of the TNH pattern and its sensitivity to tropical Pacific heating is required to improve the response to the CP El Niño in the CMIP5 models. Based on the fact that the TNH pattern is better simulated in the CMIP5 models during the EP El Niño (as shown in Figure 12a) but not well simulated during the CP El Niño (as shown in Figure 13a), it is plausible that the tropical OLR anomalies required to excite the TNH pattern may have to be of a basin-wide structure or have to be located more in the eastern-to-central Pacific. Further studies are needed.

It is also important to note that the El Niño teleconnection pattern and the wave train response can be affected by both the tropical forcing and the climatological state. This study focuses on linking the teleconnection and the wave train response to tropical SST forcing. A separate study is needed to link the teleconnections to differences in the climatological mean state.

Acknowledgments

We would like to thank three anonymous reviewers and Editor Chidong Zhang for their comments that have helped improve this paper. We also benefited from the discussions with Gerry Bell at NOAA on the analysis of the PNA and TNH patterns. This research was supported by NOAA's MAPP Program (grant A11OAR4310102) and NSF (grant AGS-1233542). This work was conducted as part of the NOAA MAPP's CMIP5 Task Force. The NCEP-NCAR Reanalysis and the NOAA interpolated OLR data are downloaded from the NOAA/ESRL PSD data portal (http://www.esrl.noaa.gov/psd), and the CMIP5 preindustrial simulations are downloaded from the CMIP5 portal (http://pcmdi9.llnl.gov/).

References

Ardanuy, P. E., and H. L. Kyle (1986), Observed perturbations of the Earth's radiation budget: A response to the El Chichón stratospheric aerosol layer?, *J. Climate Appl. Meteorol.*, *25*, 505–516, doi:10.1175/1520-0450(1986)025<0505:OPOTER>2.0.CO;2.

Ashok, K., S. K. Behera, S. A. Rao, H. Weng, and T. Yamagata (2007), El Niño Modoki and its possible teleconnection, *J. Geophys. Res.*, *112*, C11007, doi:10.1029/2006JC003798.

Barsugli, J. J., and P. D. Sardeshmukh (2002), Global atmospheric sensitivity to tropical SST anomalies throughout the Indo-Pacific basin, *J. Clim.*, *15*, 3427–3442.

Cayan, D. R., K. T. Redmond, and L. G. Riddle (1999), ENSO and hydrologic extremes in the western United States, *J. Clim.*, *12*(9), 2881–2893, doi:10.1175/1520-0442(1999)012<2881:EAHEIT>2.0.CO;2.

Chiodi, A. M., and D. E. Harrison (2013), El Niño impacts on seasonal U.S. atmospheric circulation, temperature, and precipitation anomalies: The OLR-event perspective*, *J. Clim.*, *26*(3), 822–837, doi:10.1175/JCLI-D-12-00097.1.

Dettinger, M. D., D. R. Cayan, H. F. Diaz, and D. M. Meko (1998), North–south precipitation patterns in western North America on interannual-to-decadal timescales, *J. Clim.*, *11*(12), 3095–3111, doi:10.1175/1520-0442(1998)011<3095:NSPPIW>2.0.CO;2.

Gruber, A., and A. F. Krueger (1984), The status of the NOAA outgoing longwave radiation data set, *Bull. Am. Meteorol. Soc.*, *65*, 958–962, doi:10.1175/1520-0477(1984)065<0958:TSOTNO>2.0.CO;2.

Guan, B., and S. Nigam (2008), Pacific sea surface temperatures in the twentieth century: An evolution-centric analysis of variability and trend, *J. Clim.*, *21*(12), 2790–2809, doi:10.1175/2007JCLI2076.1.

Heddinghaus, T. R., and A. F. Krueger (1981), Heddinghaus_Krueger_1981.pdf, *Mon. Weather Rev.*, *109*, 1208–1218, doi:10.1175/1520-0493(1981)109<1208:AAIVIO>2.0.CO;2.

Johnson, N. C., and S. B. Feldstein (2010), The continuum of North Pacific sea level pressure patterns: Intraseasonal, interannual, and interdecadal variability, *J. Clim.*, *23*(4), 851–867, doi:10.1175/2009JCLI3099.1.

Kalnay, E., et al. (1996), The NCEP/NCAR 40-year reanalysis project, *Bull. Am. Meteorol. Soc.*, *77*(3), 437–471, doi:10.1175/1520-0477(1996)077<0437:TNYRP>2.0.CO;2.

Kao, H.-Y., and J.-Y. Yu (2009), Contrasting eastern-Pacific and central-Pacific types of ENSO, *J. Clim.*, *22*(3), 615–632, doi:10.1175/2008JCLI2309.1.

Kiladis, G. N., and H. F. Diaz (1989), Global climatic anomalies associated with extremes in the Southern Oscillation, *J. Clim.*, *2*(9), 1069–1090, doi:10.1175/1520-0442(1989)002<1069:GCAAWE>2.0.CO;2.

Kim, S. T., and J.-Y. Yu (2012), The two types of ENSO in CMIP5 models, *Geophys. Res. Lett.*, *39*, L11704, doi:10.1029/2012GL052006.

Kug, J.-S., F.-F. Jin, and S.-I. An (2009), Two types of El Niño events: Cold tongue El Niño and warm pool El Niño, *J. Clim.*, *22*(6), 1499–1515, doi:10.1175/2008JCLI2624.1.

Larkin, N. K., and D. E. Harrison (2005), On the definition of El Niño and associated seasonal average U.S. weather anomalies, *Geophys. Res. Lett.*, *32*, L13705, doi:10.1029/2005GL022738.

Lau, K.-M., and P. H. Chan (1983), Short-term climate variability and atmospheric teleconnections from satellite-observed outgoing longwave radiation. Part I: Simultaneous relationships, *J. Atmos. Sci.*, *40*, 2735–2750, doi:10.1175/1520-0469(1983)040<2735:STCVAA>2.0.CO;2.

Lau, K.-M., and P. H. Chan (1985), Aspects of the 40–50 day oscillation during the northern winter as inferred from outgoing longwave radiation, *Mon. Weather Rev.*, *113*, 1889–1909, doi:10.1175/1520-0493(1985)113<1889:AOTDOD>2.0.CO;2.

Liang, Y.-C., M.-H. Lo, and J.-Y. Yu (2014), Asymmetric responses of land hydroclimatology to two types of El Niño in the Mississippi River Basin, *Geophys. Res. Lett.*, *41*, 582–588, doi:10.1002/2013GL058828.

Liebmann, B., and C. A. Smith (1996), LiebmannandSmith1996.pdf, *Bull. Am. Meteorol. Soc.*, *77*(6), 1275–1277.

Lin, H., G. Brunet, and R. Mo (2010), Impact of the Madden-Julian Oscillation on wintertime precipitation in Canada, *Mon. Weather Rev.*, *138*(10), 3822–3839, doi:10.1175/2010MWR3363.1.

Livezey, R. E., M. Masutani, A. Leetmaa, H. Rui, M. Ji, and A. Kumar (1997), Teleconnective response of the Pacific-North American region atmosphere to large central equatorial Pacific SST anomalies, *J. Clim.*, *10*(8), 1787–1820.

Mo, K. C. (2010), Interdecadal modulation of the impact of ENSO on precipitation and temperature over the United States, *J. Clim.*, *23*(13), 3639–3656, doi:10.1175/2010JCLI3553.1.

Mo, K. C., and R. W. Higgins (1998), Tropical convection and precipitation regimes in the western United States, *J. Clim.*, *11*(9), 2404–2423, doi:10.1175/1520-0442(1998)011<2404:TCAPRI>2.0.CO;2.

Mo, K. C., and R. E. Livezey (1986), Tropical-extratropical geopotential height teleconnections during the Northern Hemisphere winter, *Mon. Weather Rev.*, *114*, 2488–2515.

Montroy, D. L., M. B. Richman, and P. J. Lamb (1998), Observed nonlinearities of monthly teleconnections between tropical Pacific sea surface temperature anomalies and central and eastern North American precipitation, *J. Clim.*, *11*(7), 1812–1835, doi:10.1175/1520-0442(2000)013<3327:SIAEDM>2.0.CO;2.

Ropelewski, C. F., and M. S. Halpert (1986), North American precipitation and temperature patterns associated with the El Niño/Southern Oscillation (ENSO), *Mon. Weather Rev.*, *114*(12), 2352–2362.

Ropelewski, C. F., and M. S. Halpert (1989), Precipitation patterns associated with the high index phase of the Southern Oscillation, *J. Clim.*, *2*(3), 268–284.

Sheffield, J., et al. (2013), North American climate in CMIP5 experiments. Part II: Evaluation of historical simulations of intraseasonal to decadal variability, *J. Clim.*, *26*(23), 9247–9290, doi:10.1175/JCLI-D-12-00593.1.

Simmons, A. J., J. M. Wallace, and G. W. Branstator (1983), Barotropic wave propagation and instability, and atmospherric teleconnection patterns, *J. Atmos. Sci.*, *40*(6), 1363–1392.

Smith, T. M., and R. W. Reynolds (2003), Extended reconstruction of global sea surface temperatures based on COADS data (1854 – 1997), *J. Clim.*, *16*(1996), 1495–1510, doi:10.1175/1520-0442(2003)016<1495:EROGSS>2.0.CO;2.

Ting, M., and P. D. Sardeshmukh (1993), Factors determining the extratropical response to equatorial diabatic heating anomalies, *J. Atmos. Sci.*, *50*(6), 907–918.

Wallace, J. M., and D. S. Gutzler (1981), Teleconnections in the geopotential height field during the Northern Hemisphere winter, *Mon. Weather Rev.*, *109*(4), 784–812, doi:10.1175/1520-0493(1981)109<0784:TITGHF>2.0.CO;2.

Weng, H., S. K. Behera, and T. Yamagata (2009), Anomalous winter climate conditions in the Pacific rim during recent El Niño Modoki and El Niño events, *Clim. Dyn.*, *32*(5), 663–674, doi:10.1007/s00382-008-0394-6.

Xu, K., C. Zhu, and J. He (2013), Two types of El Niño-related Southern Oscillation and their different impacts on global land precipitation, *Adv. Atmos. Sci.*, *30*(6), 1743–1757, doi:10.1007/s00376-013-2272-3.1.Introduction.

Yu, J.-Y., and H.-Y. Kao (2007), Decadal changes of ENSO persistence barrier in SST and ocean heat content indices: 1958–2001, *J. Geophys. Res.*, *112*, D13106, doi:10.1029/2006JD007654.

Yu, J.-Y., and S. T. Kim (2010), Three evolution patterns of Central-Pacific El Niño, *Geophys. Res. Lett.*, *37*, L08706, doi:10.1029/2010GL042810.

Yu, J.-Y., and Y. Zou (2013), The enhanced drying effect of Central-Pacific El Niño on US winter, *Environ. Res. Lett.*, *8*(1), 014019, doi:10.1088/1748-9326/8/1/014019.

Yu, J.-Y., M.-M. Lu, and S. T. Kim (2012a), A change in the relationship between tropical central Pacific SST variability and the extratropical atmosphere around 1990, *Environ. Res. Lett.*, *7*(3), 034025, doi:10.1088/1748-9326/7/3/034025.

Yu, J.-Y., Y. Zou, S. T. Kim, and T. Lee (2012b), The changing impact of El Niño on US winter temperatures, *Geophys. Res. Lett.*, *39*, L15702, doi:10.1029/2012GL052483.